

Hydroborate Solid-State Lithium Battery with High-Voltage NMC811 Cathode

Hugo Braun,[†] Ryo Asakura,[†] Arndt Remhof,* and Corsin Battaglia



Cite This: *ACS Energy Lett.* 2024, 9, 707–714



Read Online

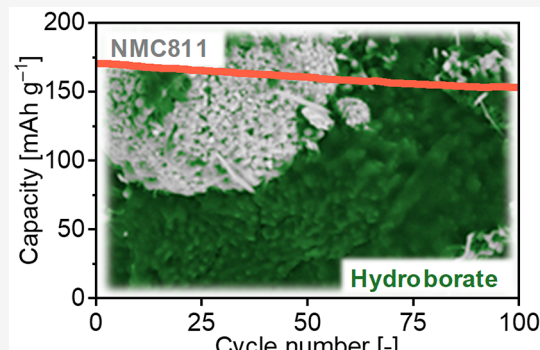
ACCESS |

Metrics & More

Article Recommendations

Supporting Information

ABSTRACT: Hydroborate solid electrolytes offer high ionic conductivity and are stable in contact with alkali metal anodes but are challenging to integrate into batteries with high-voltage cathodes. Here, we demonstrate stable dis-/charge cycling of solid-state Li batteries combining a $\text{Li}_3(\text{CB}_{11}\text{H}_{12})_2(\text{CB}_9\text{H}_{10})$ hydroborate electrolyte with a 4 V-class $\text{LiNi}_{0.8}\text{Mn}_{0.1}\text{Co}_{0.1}\text{O}_2$ (NMC811) cathode, exploiting the enhanced kinetic stability of the $\text{LiCB}_{11}\text{H}_{12}$ -rich and $\text{LiCB}_9\text{H}_{10}$ -poor electrolyte composition. Cells with Li metal and InLi anodes achieve a discharge capacity at C/10 of $\sim 145 \text{ mAh g}^{-1}$ at room temperature and $\sim 175 \text{ mAh g}^{-1}$ at 60 °C. InLi cells retain 98% of their initial discharge capacity after 100 cycles at C/5 and 70% after 1000 cycles at C/2. Capacity retentions of 97% after 100 cycles at C/5 and 75% after 350 cycles at C/2 are also achieved with a graphite anode without any excess Li. The energy density per cathode composite weight of 460 Wh kg⁻¹ is on par with the best solid-state batteries reported to date.



L-ion batteries are indispensable for a range of applications, from portable electronics to electric mobility. Solid-state batteries with solid electrolytes are expected to expand the energy density beyond the limits of current Li-ion batteries,^{1–5} replace their flammable^{6,7} liquid organic electrolytes with safer nonflammable alternatives, and enable faster charging.⁸ The most heavily investigated solid electrolyte classes are polymers, sulfides, oxides, and halides. Each of them has its own advantages and disadvantages. Polymers are flexible and easy to process, but their Li-ion conductivity, typically $< 1 \text{ mS cm}^{-1}$ at room temperature, and thermal and electrochemical stability are not yet sufficient to establish a competitive battery technology.^{9–13} Sulfides can reach Li-ion conductivities above 10 mS cm^{-1} and are mechanically soft.⁸ However, their low chemical and electrochemical stability still raises safety concerns.^{14–19} Oxides exhibit Li-ion conductivities of up to $\sim 1 \text{ mS cm}^{-1}$ with high thermal and electrochemical stability, but are mechanically rigid, making it challenging to accommodate volume changes of electrode materials during dis-/charge cycling.^{8,20–23} Halides feature Li-ion conductivities of $> 1 \text{ mS cm}^{-1}$ and high oxidative stability, but are typically unstable against Li metal.^{24–27}

In contrast, hydroborates, a specific type of complex metal hydrides, have only recently emerged as solid electrolytes and offer distinct advantages.^{28,29} Hydroborates combine high Li- and Na-ion conductivity at room temperature with excellent reductive stability in contact with Li and Na metal and

relatively high oxidative stability.^{30–33} Furthermore, hydroborates typically exhibit a low crystallographic density of only $1.0\text{--}1.2 \text{ g cm}^{-3}$ ^{34–36} are mechanically soft, and can be crystallized from solution, which may facilitate large-scale production.^{28,37} The Na hydroborates typically exhibit higher ionic conductivities up to 70 mS cm^{-1} at room temperature³⁸ than their Li analogues, which reach up to 6.7 mS cm^{-1} .^{31,39} Some of us successfully demonstrated stable room temperature cycling of a hydroborate solid-state Na battery with a 4 V-class $\text{Na}_3(\text{VOPO}_4)_2\text{F}$ cathode and a Na metal anode, delivering $\sim 100 \text{ mAh g}^{-1}$ upon discharge.³²

However, stable long-term cycling of a high-capacity 4 V-class cathode such as $\text{LiNi}_{0.8}\text{Mn}_{0.1}\text{Co}_{0.1}\text{O}_2$ (NMC811) delivering up to 200 mAh g^{-1} has not yet been demonstrated. Most previous studies have focused on optimizing the ionic conductivity of Li hydroborates, reaching so far the highest value of 6.7 mS cm^{-1} for a 3:7 mixture of $\text{LiCB}_{11}\text{H}_{12}$ and $\text{LiCB}_9\text{H}_{10}$.³¹ Systematic efforts to investigate and enhance the oxidative stability of Li hydroborates are lacking, which is why stable dis-/charge cycling of cells based on these Li hydroborates has so far been demonstrated exclusively for

Received: October 6, 2023

Revised: December 18, 2023

Accepted: December 19, 2023

cells with low-voltage cathodes like S^{31,40} or TiS₂^{30,39,41,42}. Attempts to enable the integration of 4 V-class cathodes including a LiNbO₃ protective layer⁴³ or the use of a kinetically more stable, but less conductive Li₂B₁₂H₁₂–Al₂O₃ electrolyte⁴¹ have so far resulted only in poor capacity retention (<80% after 20 cycles), suggesting that interface stability is still insufficient.

In this study, we reconsidered the mixtures of LiCB₁₁H₁₂ and LiCB₉H₁₀. In particular, we evaluate the oxidative stability as a function of the LiCB₁₁H₁₂-to-LiCB₉H₁₀ ratio. We find that the Li₃(CB₁₁H₁₂)₂(CB₉H₁₀) composition with a 2:1 ratio offers significantly higher oxidative stability (~3.9 V vs Li⁺/Li) than the LiCB₉H₁₀-rich 1:2 composition (~3.6 V vs Li⁺/Li), while maintaining a high Li-ion conductivity (1.5 mS cm⁻¹ at room temperature and 29.4 mS cm⁻¹ at 60 °C). The Li₃(CB₁₁H₁₂)₂(CB₉H₁₀) electrolyte is successfully integrated with a high-voltage NMC811 cathode synthesized in-house⁴⁴ in combination with Li, InLi, and graphite anodes (Figure 1).

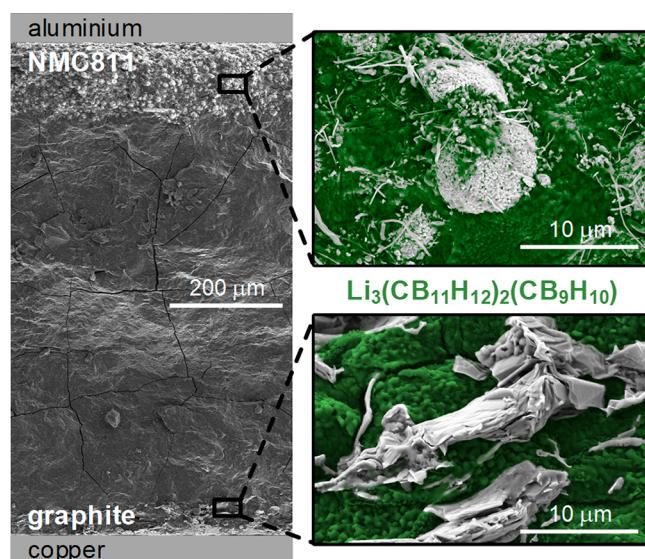


Figure 1. SEM images of the cell cross-section with schematically added current collectors: aluminum current collector, cathode composite with NMC811 and solid electrolyte, solid electrolyte separator, anode composite with graphite and solid electrolyte, and copper current collector (top to bottom). Enlarged views show SEM images of NMC811 particles and vapor-grown carbon fibers (top) and graphite flakes (bottom) embedded in Li₃(CB₁₁H₁₂)₂(CB₉H₁₀) solid electrolyte (false-colored green). Current collectors are not drawn to scale.

Excellent cycling stability over several hundred dis-/charge cycles is achieved with InLi and graphite anodes, demonstrating the advantages of the LiCB₁₁H₁₂-rich and LiCB₉H₁₀-poor 2:1 composition. Importantly, our results bring the hydroborates to a performance level comparable to the best solid electrolytes reported so far. Unlike many previous reports, we achieve this by using the very same solid electrolyte in the cathode composite, as the separator layer, and in contact with the anode.

■ TRADE-OFF BETWEEN IONIC CONDUCTIVITY AND OXIDATIVE STABILITY

To explore Li-hydroborate-based solid electrolytes that combine high ionic conductivity with high electrochemical oxidative stability, we first revisit the mixed-anion *closocarbaborates* of LiCB₁₁H₁₂ and LiCB₉H₁₀. Figure 2a shows the temperature-dependent ionic conductivity of ball-milled LiCB₁₁H₁₂, LiCB₉H₁₀, and their mixtures with molar ratios of 2:1, 1:1, 1:2, and 1:4. All mixtures exhibit higher Li-ion conductivity than either of the two individual components, resulting from the lowering of the phase transition temperature upon mixing as witnessed by differential scanning calorimetry (DSC) shown in Figure S1, analogous to the case of mixed-anion Na hydroborates.^{38,45,46} For ratios of 1:1, 1:2, and 1:4, the phase transition is no longer apparent in the DSC traces, even if the resulting phases are not single phase at room temperature as evidenced by X-ray diffraction (XRD) patterns in Figure S2, which agrees well with a previous study.³⁹ The XRD patterns shown in Figure S2 indicate that the 2:1 mixture is isostructural with LiCB₁₁H₁₂, while the other mixtures contain multiple phases dominated by the LiCB₉H₁₀ phase. This suggests that the larger [CB₁₁H₁₂]⁻-anion-derived face-centered cubic lattice can accommodate the smaller [CB₉H₁₀]⁻ anions, while the reverse is not possible.

Notably, while the ionic conductivity of LiCB₁₁H₁₂ and LiCB₉H₁₀ at 25 °C is only ~0.1 mS cm⁻¹, that of their mixtures at 25 °C exceeds 1.5 mS cm⁻¹ for every mixing ratio, which for some ratios is higher than the previously reported values.³⁹ This can be attributed to the difference in ball-milling conditions because a high-energy ball mill was employed in this study, while a planetary ball mill was employed in the previous study. At 60 °C, the 2:1 LiCB₁₁H₁₂–LiCB₉H₁₀ mixture exhibits the highest conductivity of 29.4 mS cm⁻¹ among the mixing ratios studied, thanks to the lowered phase-transition temperature of LiCB₁₁H₁₂ by mixing with LiCB₉H₁₀.

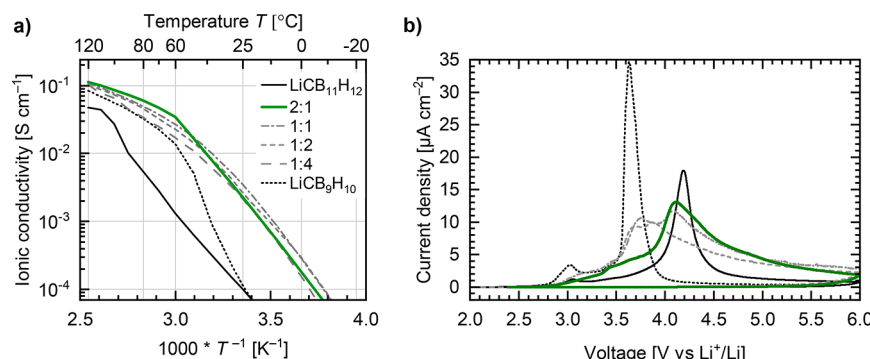


Figure 2. (a) Arrhenius plot of the ionic conductivity measured between –20 and 120 °C during the second cooling and (b) cyclic voltammograms between 2.0 and 6.0 V vs Li⁺/Li at a scan rate of 10 μV s⁻¹ at 60 °C for LiCB₁₁H₁₂, LiCB₉H₁₀, and their mixtures with molar ratios of 2:1, 1:1, 1:2, and 1:4.

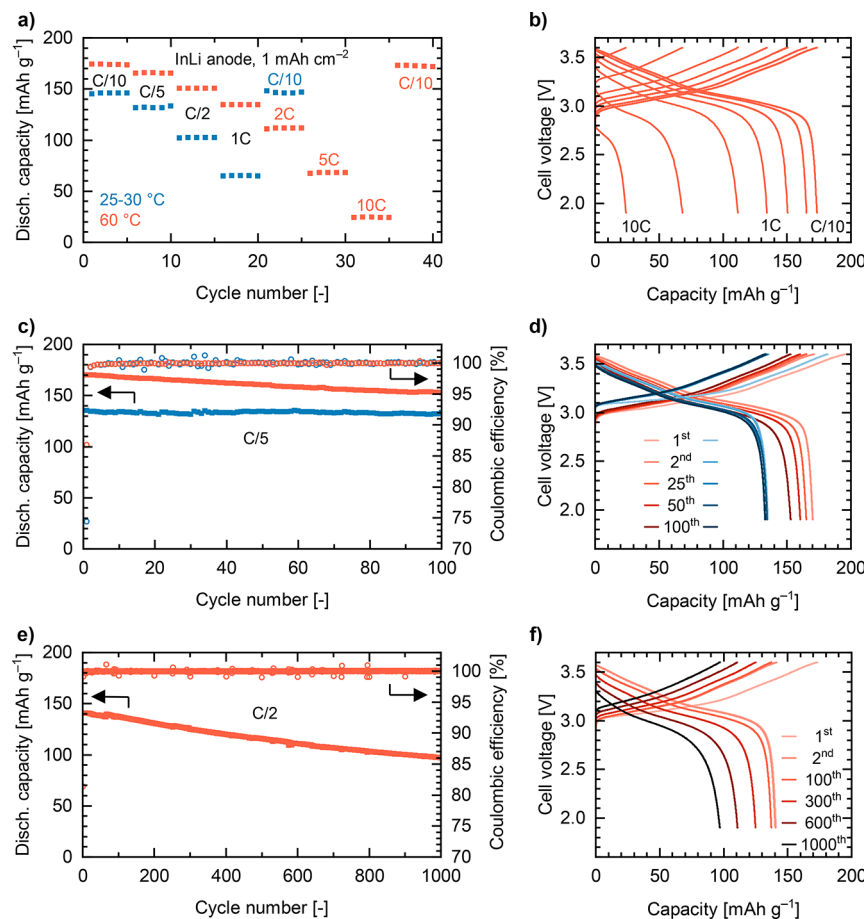


Figure 3. Solid-state cell performance at room temperature (blue) and at 60 °C (red) with $\text{Li}_3(\text{CB}_{11}\text{H}_{12})_2(\text{CB}_9\text{H}_{10})$ solid electrolyte, NMC811 composite cathode, and InLi anode, in terms of (a, b) rate capability, (c, d) cycling stability at C/5, and (e, f) cycling stability at C/2. The discharge capacity is normalized to the weight of the cathode active material in the lithiated state.

These conductivity data suggest that all mixtures can function as highly conductive Li-ion solid electrolytes over a wide temperature range, from room temperature to elevated temperatures.

Subsequently, the electrochemical oxidative stability is examined by voltammetric methods to identify solid electrolytes that are compatible with high-voltage cathodes. This method has been shown to yield experimental stability values in close agreement with thermodynamic stability values obtained from first-principles calculations.⁴⁷ Figure 2b shows the cyclic voltammograms of $\text{LiCB}_{11}\text{H}_{12}$, $\text{LiCB}_9\text{H}_{10}$, and their mixtures between 2.0 and 6.0 V vs Li^+/Li at a scan rate of 10 $\mu\text{V s}^{-1}$ at 60 °C. All samples show a tiny initial oxidation peak at ~ 3.0 V vs Li^+/Li , which is commonly observed in other *closو-hydroborates* and is not related to subsequent oxidation.^{32,47} When we compare the onset potential of the main electrochemical oxidation of the *closو-carbaborate* anions, $[\text{CB}_{11}\text{H}_{12}]^-$ shows the highest value of ~ 4.0 V vs Li^+/Li , while $[\text{CB}_9\text{H}_{10}]^-$ shows the lowest value of 3.55 V vs Li^+/Li . The oxidation peaks in the mixtures consist of a linear combination of peaks derived from $[\text{CB}_{11}\text{H}_{12}]^-$ and $[\text{CB}_9\text{H}_{10}]^-$ anions, with peak intensities roughly depending on the mixing ratio. Our results thus suggest that the apparent electrochemical oxidative stability of the hydroborate anion mixtures can be increased kinetically by employing $\text{LiCB}_{11}\text{H}_{12}$ -rich electrolyte compositions, i.e. by enriching the electrolyte with the thermodynamically more stable $[\text{CB}_{11}\text{H}_{12}]^-$ anions.²⁹

In particular, the 2:1 mixture contains a non-negligible amount of $[\text{CB}_9\text{H}_{10}]^-$ but succeeds in suppressing the oxidation peak derived from $[\text{CB}_9\text{H}_{10}]^-$ in Figure 2b. We attribute this to the fact that the major component in the mixture is the thermodynamically more stable $[\text{CB}_{11}\text{H}_{12}]^-$ and the thermodynamically less stable $[\text{CB}_9\text{H}_{10}]^-$ is incorporated into the face-centered cubic $\text{LiCB}_{11}\text{H}_{12}$ structure (see Figure S2). This is significant because the former studies on the $\text{LiCB}_{11}\text{H}_{12}$ - $\text{LiCB}_9\text{H}_{10}$ mixtures focused on a $\text{LiCB}_9\text{H}_{10}$ -rich phase, which limits the oxidative stability to ~ 3.6 V vs Li^+/Li for the 1:2 mixture (Figure 2b) and hence limits the selection of cathode active materials (e.g., to S or TiS_2).^{31,39} In contrast, the higher oxidative stability of the 2:1 mixture up to ~ 3.9 V vs Li^+/Li opens up the possibility to use higher-voltage cathodes. This mixing ratio possesses a good balance between ionic conductivity and electrochemical oxidative stability and will be referred to as $\text{Li}_3(\text{CB}_{11}\text{H}_{12})_2(\text{CB}_9\text{H}_{10})$.

■ INTEGRATION INTO ALL-SOLID-STATE BATTERIES

The $\text{Li}_3(\text{CB}_{11}\text{H}_{12})_2(\text{CB}_9\text{H}_{10})$ solid electrolyte is combined with an in-house developed, high-voltage NMC811 cathode^{44,48} and three different anodes, namely Li metal, InLi, and graphite. The cathode active material is bulk-doped with 0.3 mol % Ti and surface-coated with 0.6 mol % TiO_2 , as described elsewhere.⁴⁴ A schematic of the NMC811-graphite cell cross-section based on SEM images is displayed in Figure 1. The NMC811 composite cathode with an areal capacity of

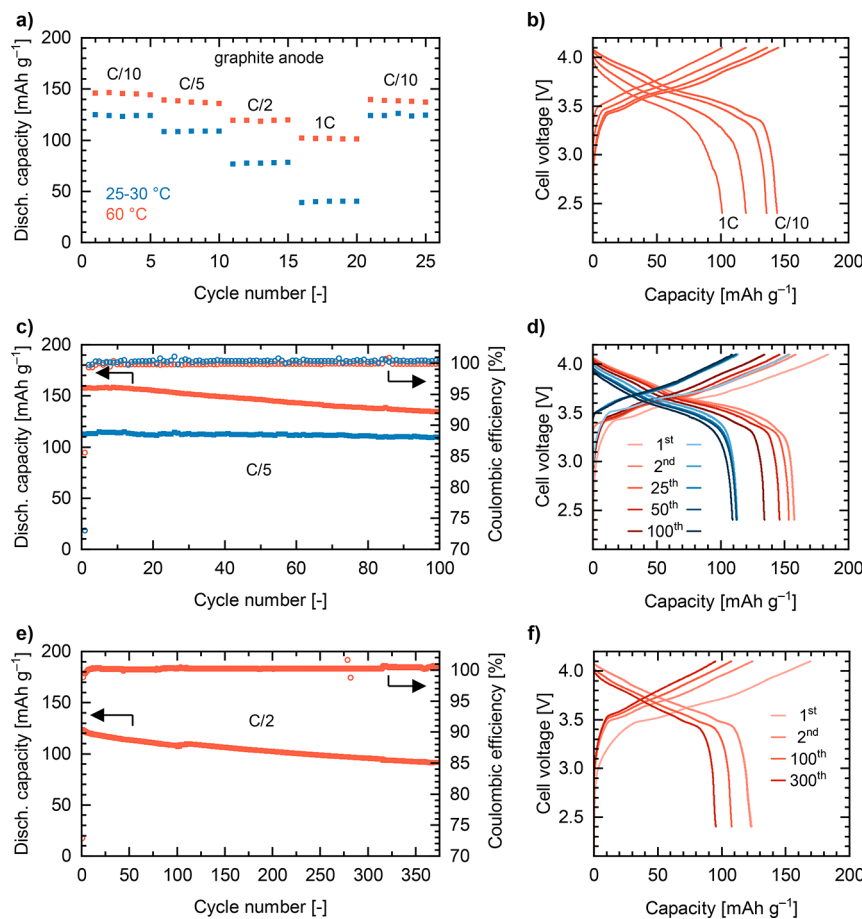


Figure 4. Solid-state cell performance at room temperature (blue) and at 60 °C (red) with $\text{Li}_3(\text{CB}_{11}\text{H}_{12})_2(\text{CB}_9\text{H}_{10})$ solid electrolyte, NMC811 composite cathode, and graphite composite anode in terms of (a, b) rate capability, (c, d) cycling stability at C/5, and (e, f) cycling stability at C/2.

0.34 mAh cm⁻² delivers a high reversible discharge capacity at C/10 of ~145 mAh g⁻¹ and ~175 mAh g⁻¹ at room temperature and 60 °C, respectively, when cycled to an upper cutoff voltage of 4.2 V vs a Li metal anode (Figure S3). However, even at 60 °C, these cells short-circuit within the first 20 cycles due to penetration of Li metal through the solid electrolyte (Figure S3c).

Short circuits are prevented with an InLi alloy anode. NMC811-InLi cell cycling results are shown in Figures 3a and 3b, delivering an initial discharge capacity at C/10 of 145 mAh g⁻¹ and 175 mAh g⁻¹ at room temperature and 60 °C, respectively. At 2 C, the cell retains more than 100 mAh g⁻¹ and it can be charged and discharged at 10 C, equivalent to 10 mA cm⁻² and 1700 mA g⁻¹, without affecting the capacity at lower rates (i.e., when returning to C/10). In Figures 3c and 3d, we demonstrate remarkable cycling stability with 98% and 90% capacity retention after 100 cycles at C/5 at room temperature and 60 °C, respectively. The Coulombic efficiency is 75% and 87% for the first cycle, respectively, and >99% for all subsequent cycles, indicating that the interfaces are stabilized after the first cycle.⁴⁹ A higher cutoff voltage of 4.3 V instead of 4.2 V vs Li⁺/Li slightly increases the initial capacity at the cost of faster fading (Figure S4), which is why we choose an upper cutoff voltage of 3.6 V vs In/InLi (4.222 V vs Li⁺/Li) to maintain long-term stability. Even after 1000 cycles at C/2, 70% of the initial discharge capacity is still

available (Figures 3e and 3f), and 54% after 2000 cycles (Figure S13).

While the rate capability and cycling stability with the InLi anode are promising, the resulting cell voltage is relatively low (0.622 V lower than with a Li metal anode). In addition, In is not sufficiently abundant and InLi has only about half the specific capacity of graphite (372 mAh g⁻¹), considering the limit of 45 at% Li in the InLi alloy to stay on the 0.622 V plateau vs Li⁺/Li.^{50,51} In addition, the InLi anode provides a nearly infinite reservoir of Li that can compensate for the losses of active Li in the cell. Therefore, we investigate full cells with a graphite anode, which is commercially relevant, enables a cell voltage only 0.1 V lower than with Li metal anode,⁵⁰ and does not provide any excess Li, imposing an even more stringent condition on the capacity retention.

The corresponding cells with the same amount of NMC811 cathode active material possess a discharge capacity of 125 mAh g⁻¹ and 150 mAh g⁻¹ at room temperature and 60 °C, when cycled to an upper cutoff voltage of 4.1 V vs a graphite anode (~4.2 V vs Li⁺/Li) (Figure 4a and Figure S5). Importantly, we utilize almost all of the theoretical capacity of graphite (Figure S6), and no more than 5–10% additional anode capacity is needed to balance the cell (Figure S7). Compared to cells with the InLi anode, the discharge capacity is about 20–25 mAh g⁻¹ lower. The difference is independent of the C rate and temperature (Figure S8). Moreover, the cell impedance (Figure S9), the dis-/charge overpotentials (Figure

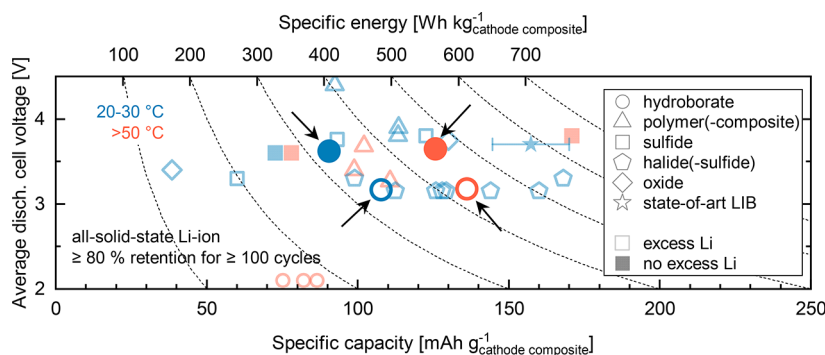


Figure 5. Performance of stable state-of-the-art solid-state Li batteries reported in the literature, in terms of average discharge cell voltage, specific discharge capacity, and specific energy, normalized by the cathode composite weight in the lithiated state. Only solid-state cells with a capacity retention of at least 80% after 100 cycles are considered. The shape of the symbol indicates the type of solid electrolyte: hydroborates (circles),^{30,39,42} polymer and polymer composites (triangles),^{57–61} sulfides (squares),^{52,53,62–64} halides and halide-sulfide bilayer (pentagons),^{65–71} and oxides (diamonds).^{72,73} Empty symbols indicate cells containing excess Li (oversized Li metal anodes or InLi alloy anodes). Full symbols indicate cells without excess Li (graphite and Ag–C anodes). For comparison, the approximate performance of a state-of-the-art liquid electrolyte Li-ion battery (LIB) is indicated (star), calculated based on NMC with 170–200 mAh g⁻¹ and accounting for the weight of the liquid electrolyte.⁷⁴ The symbols highlighted with arrows correspond to the values obtained in this work. The values obtained from the literature are summarized in Tables S1–S5.

S10) and the extra capacity obtained by a constant-voltage step (Figure S11) are very similar between cells with InLi and graphite anodes. For these reasons, we rule out a larger cell resistance or slower kinetics in graphite cells as the cause of the lower discharge capacity. Rather, we consider a lower amount of reversibly active Li for the graphite cells, which can be attributed to the following two phenomena. First, not all of the Li intercalated into the graphite during the first charge can be subsequently deintercalated (Figure S6), which accounts for up to 15 mAh g⁻¹. Second, if an interphase forms between the solid electrolyte and the NMC811 particles upon charge, the Li consumed in this process cannot be replaced during discharge in the case of a graphite anode, because there is no excess Li available as in the case of the Li and InLi anode.

The high capacity retention of the cells with the graphite anode (up to 97% after 100 cycles, as shown in Figures 4c and 4d, and 75% after 350 cycles, as shown in Figures 4e and 4f), in which no excess Li is available, is clear evidence that Li is not continuously consumed, but instead stable passivating interfaces are formed. Based on the high capacity retention without excess Li, stable dis-/charge cycling up to 4.2 V vs Li⁺/Li is possible, which is beyond the stability of the Li₃(CB₁₁H₁₂)₂(CB₉H₁₀) electrolyte (~3.9 V vs Li⁺/Li, Figure 2b). Factors contributing to this stable dis-/charge cycling could be (i) the formation of hydroborate anion dimers with higher stability at the interface³² and/or (ii) the TiO₂ coating on the NMC811 surface. More research is needed in the future to clarify the interface passivation. Overall, we can conclude that the increased stability of the cathode–solid electrolyte interface results in excellent capacity retention, even without any excess Li.

Figure 5 compares our solid-state cells to cells reported in the literature, which have demonstrated a capacity retention of at least 80% after 100 cycles. Compared to all the previous hydroborate-based solid-state Li batteries (circles), our cells (marked with arrows) exhibit by far the best combination between high cell voltage, high cathode-specific capacity, and cycling stability. More than 80% capacity retention after 100 cycles for Li hydroborate solid-state batteries has previously only been achieved with low-voltage TiS₂ cathodes.^{30,39,42} More importantly, the hydroborate-based battery reported in

this work is among the leading solid-state Li cells in terms of specific energy per cathode composite weight. For example, the 460 Wh kg⁻¹ obtained in this work with the Li₃(CB₁₁H₁₂)₂(CB₉H₁₀) electrolyte compares well with the 466 Wh kg⁻¹ achieved with a Li₆PS₅Cl electrolyte.⁵² Finally, if we consider full cells without excess Li (filled symbols), we know of only one other report, using an Ag–C composite anode, surpassing our cell.⁵³ For practical applications, the energy density at the cell level is decisive. The crystallographic density of *closo*-hydroborates as reported in the ICSD structure database (Li₂B₁₂H₁₂, 1.18 g cm⁻³; Li₂B₁₀H₁₀, 1.03 g cm⁻³; NaCB₉H₁₀, 1.14 g cm⁻³)^{34–36} is significantly lower than the density of the commonly used oxide (Li₇La₃Zr₂O₁₂: 5.12 g cm⁻³),⁵⁴ halide (Li₃InCl₆: 2.71 g cm⁻³),⁵⁵ and sulfide electrolytes (Li₆PS₅Cl: 1.86 g cm⁻³).⁵⁶ Therefore, we expect a competitive gravimetric energy density at the cell level for an optimized hydroborate-based cell architecture.

To conclude, we demonstrate stable cycling of hydroborate-based solid-state batteries with a state-of-the-art 4 V-class NMC811 cathode. The interface stability between the hydroborate electrolyte and the NMC811 cathode is kinetically improved by using a LiCB₁₁H₁₂-rich and LiCB₉H₁₀-poor electrolyte composition, which maintains a high Li-ion conductivity. While Li metal penetration remains an issue to be addressed in future studies, cells with InLi and graphite anodes feature a remarkable capacity retention of 98% and 97% after 100 cycles at room temperature, confirming the excellent properties of the hydroborate electrolyte in combination with the NMC811 during dis-/charge cycling. With an energy density per cathode composite weight of 460 Wh kg⁻¹, our cells are on par with the best solid-state batteries reported to date.

In the future, the cell should be developed toward an industrial prototype by reducing the separator thickness from 900 μm to 20–25 μm, increasing the areal capacity from 1 mAh cm⁻² to 4–5 mAh cm⁻², improving the rate capability at room temperature, defining strategies to suppress Li metal penetration from the anode to the cathode, and reducing the costs associated with hydroborate anion synthesis.

■ ASSOCIATED CONTENT

SI Supporting Information

The Supporting Information is available free of charge at <https://pubs.acs.org/doi/10.1021/acsenergylett.3c02117>.

Experimental section (material preparation and characterization, cell assembly and electrochemical characterization) as well as supplemental figures and tables showing the thermal and structural characterization of the solid electrolyte, cycling stability of NMC811-Li metal cells, the capacity at higher cutoff voltages, the capacity of the graphite used, a comparison of the discharge capacities of the individual cells with InLi anode and graphite anode, Nyquist plots of potentiostatic electrochemical impedance spectroscopy, time evolution of cell voltage vs Li⁺/Li, cycling stability up to 2000 cycles, and a literature overview of the performance parameters of solid-state Li batteries featuring currently discussed solid electrolytes of various material classes in tabular form ([PDF](#))

■ AUTHOR INFORMATION

Corresponding Author

Arndt Remhof — Empa, Swiss Federal Laboratories for Materials Science and Technology, 8600 Dübendorf, Switzerland; Institut für Anorganische und Analytische Chemie, Albert-Ludwigs-Universität Freiburg, 79104 Freiburg, Germany;  orcid.org/0000-0002-8394-9646; Email: arndt.remhof@empa.ch

Authors

Hugo Braun — Empa, Swiss Federal Laboratories for Materials Science and Technology, 8600 Dübendorf, Switzerland; Institut für Anorganische und Analytische Chemie, Albert-Ludwigs-Universität Freiburg, 79104 Freiburg, Germany;  orcid.org/0000-0001-9903-5614

Ryo Asakura — Empa, Swiss Federal Laboratories for Materials Science and Technology, 8600 Dübendorf, Switzerland;  orcid.org/0000-0002-9264-9493

Corsin Battaglia — Empa, Swiss Federal Laboratories for Materials Science and Technology, 8600 Dübendorf, Switzerland; Departement of Information Technology and Electrical Engineering, ETH Zurich, 8092 Zurich, Switzerland;  orcid.org/0000-0002-5003-1134

Complete contact information is available at:
<https://pubs.acs.org/10.1021/acsenergylett.3c02117>

Author Contributions

¹Hugo Braun and Ryo Asakura contributed equally

Notes

The authors declare no competing financial interest.

■ ACKNOWLEDGMENTS

The authors would like to thank Wengao Zhao and Francesco Bizzotto for preparing the NMC cathode active material, Seyedhosein Payandeh for carrying out Rietveld refinement and Edouard Querel for help with acquiring SEM images.

■ REFERENCES

- (1) Pacios, R.; Villaverde, A.; Martínez-Ibañez, M.; Casas-Cabañas, M.; Agusse, F.; Kvasha, A. Roadmap for Competitive Production of Solid-State Batteries: How to Convert a Promise into Reality. *Adv. Energy Mater.* **2023**, *13*, 2301018.
- (2) European Commission. *Roadmap on Advanced Materials for Batteries*; 2021; <https://energy.ec.europa.eu/system/files/2021-12/vol-3-008-2.pdf> (accessed 2023/07/07).
- (3) Schmaltz, T.; Wicke, T.; Weymann, L.; Voß, P.; Neef, C.; Thielmann, A. *Solid-State Battery Roadmap 2035+*; 2022; https://www.isi.fraunhofer.de/content/dam/isi/dokumente/cct/2022/SSB_Roadmap.pdf (accessed 2023/07/07).
- (4) Pasta, M.; Armstrong, D.; Brown, Z. L.; Bu, J.; Castell, M. R.; Chen, P.; Cocks, A.; Corr, S. A.; Cussen, E. J.; Darnbrough, E.; et al. 2020 roadmap on solid-state batteries. *J. Phys.: Energy* **2020**, *2* (3), 032008.
- (5) Janek, J.; Zeier, W. G. A solid future for battery development. *Nat. Energy* **2016**, *1* (9), 16141.
- (6) Wang, J.; Zheng, Q.; Fang, M.; Ko, S.; Yamada, Y.; Yamada, A. Concentrated Electrolytes Widen the Operating Temperature Range of Lithium-Ion Batteries. *Adv. Sci.* **2021**, *8* (18), 2101646.
- (7) Wu, Y.; Wang, S.; Li, H.; Chen, L.; Wu, F. Progress in thermal stability of all-solid-state-Li-ion-batteries. *InfoMat* **2021**, *3* (8), 827–853.
- (8) Janek, J.; Zeier, W. G. Challenges in speeding up solid-state battery development. *Nat. Energy* **2023**, *8* (3), 230–240.
- (9) Zhao, X.; Wang, C.; Liu, H.; Liang, Y.; Fan, L.-Z. A Review of Polymer-based Solid-State Electrolytes for Lithium-Metal Batteries: Structure, Kinetic, Interface Stability, and Application. *Batteries Supercaps* **2023**, *6* (4), No. e202200502.
- (10) Zhang, X.; Daigle, J.-C.; Zaghib, K. Comprehensive Review of Polymer Architecture for All-Solid-State Lithium Rechargeable Batteries. *Materials* **2020**, *13* (11), 2488.
- (11) Mindemark, J.; Lacey, M. J.; Bowden, T.; Brandell, D. Beyond PEO—Alternative host materials for Li⁺-conducting solid polymer electrolytes. *Prog. Polym. Sci.* **2018**, *81*, 114–143.
- (12) Zhao, Y.; Wang, L.; Zhou, Y.; Liang, Z.; Tavajohi, N.; Li, B.; Li, T. Solid Polymer Electrolytes with High Conductivity and Transference Number of Li Ions for Li-Based Rechargeable Batteries. *Adv. Sci.* **2021**, *8* (7), 2003675.
- (13) Ngai, K. S.; Ramesh, S.; Ramesh, K.; Juan, J. C. A review of polymer electrolytes: fundamental, approaches and applications. *Ionics* **2016**, *22* (8), 1259–1279.
- (14) Culver, S. P.; Koerver, R.; Zeier, W. G.; Janek, J. On the Functionality of Coatings for Cathode Active Materials in Thiophosphate-Based All-Solid-State Batteries. *Adv. Energy Mater.* **2019**, *9* (24), 1900626.
- (15) Liang, J.; Li, X.; Wang, C.; Kim, J. T.; Yang, R.; Wang, J.; Sun, X. Current Status and Future Directions in Environmental Stability of Sulfide Solid-State Electrolytes for All-Solid-State Batteries. *Energy Mater. Adv.* **2023**, *4*, 0021.
- (16) Wang, C.; Adair, K.; Sun, X. All-Solid-State Lithium Metal Batteries with Sulfide Electrolytes: Understanding Interfacial Ion and Electron Transport. *Acc. Mater. Res.* **2022**, *3* (1), 21–32.
- (17) Suci, W. G.; Aliwarga, H. K.; Azinuddin, Y. R.; Setyawati, R. B.; Stulasti, K. N. R.; Purwanto, A. Review of various sulfide electrolyte types for solid-state lithium-ion batteries. *Open Eng.* **2022**, *12* (1), 409–423.
- (18) Byeon, Y.-W.; Kim, H. Review on Interface and Interphase Issues in Sulfide Solid-State Electrolytes for All-Solid-State Li-Metal Batteries. *Electrochim.* **2021**, *2* (3), 452–471.
- (19) Zheng, J.; Zhu, X.; Wang, L.; Lu, J.; Wu, T. Insights into interfacial physiochemistry in sulfide solid-state batteries: a review. *Mater. Chem. Front.* **2023**, *7*, 4810.
- (20) Ren, Y.; Danner, T.; Moy, A.; Finsterbusch, M.; Hamann, T.; Dippell, J.; Fuchs, T.; Müller, M.; Hoft, R.; Weber, A.; et al. Oxide-Based Solid-State Batteries: A Perspective on Composite Cathode Architecture. *Adv. Energy Mater.* **2023**, *13* (1), 2201939.
- (21) Luo, W.; Gong, Y.; Zhu, Y.; Li, Y.; Yao, Y.; Zhang, Y.; Fu, K.; Pastel, G.; Lin, C.-F.; Mo, Y.; et al. Reducing Interfacial Resistance between Garnet-Structured Solid-State Electrolyte and Li-Metal Anode by a Germanium Layer. *Adv. Mater.* **2017**, *29* (22), 1606042.

- (22) Kravchyk, K. V.; Karabay, D. T.; Kovalenko, M. V. On the feasibility of all-solid-state batteries with LLZO as a single electrolyte. *Sci. Rep.* **2022**, *12* (1), 1177.
- (23) Kim, S.; Kim, J.-S.; Miara, L.; Wang, Y.; Jung, S.-K.; Park, S. Y.; Song, Z.; Kim, H.; Badding, M.; Chang, J.; et al. High-energy and durable lithium metal batteries using garnet-type solid electrolytes with tailored lithium-metal compatibility. *Nat. Commun.* **2022**, *13* (1), 1883.
- (24) Wang, C.; Liang, J.; Kim, J. T.; Sun, X. Prospects of halide-based all-solid-state batteries: From material design to practical application. *Sci. Adv.* **2022**, *8* (36), No. eadc9516.
- (25) Li, X.; Liang, J.; Yang, X.; Adair, K. R.; Wang, C.; Zhao, F.; Sun, X. Progress and perspectives on halide lithium conductors for all-solid-state lithium batteries. *Energy Environ. Sci.* **2020**, *13* (5), 1429–1461.
- (26) Tuo, K.; Sun, C.; Liu, S. Recent Progress in and Perspectives on Emerging Halide Superionic Conductors for All-Solid-State Batteries. *Electrochem. Energy Rev.* **2023**, *6* (1), 17.
- (27) Nikodimos, Y.; Su, W.-N.; Hwang, B. J. Halide Solid-State Electrolytes: Stability and Application for High Voltage All-Solid-State Li Batteries. *Adv. Energy Mater.* **2023**, *13* (3), 2202854.
- (28) Duchêne, L.; Remhof, A.; Hagemann, H.; Battaglia, C. Status and prospects of hydroborate electrolytes for all-solid-state batteries. *Energy Storage Mater.* **2020**, *25*, 782–794.
- (29) Asakura, R.; Remhof, A.; Battaglia, C. Hydroborate-Based Solid Electrolytes for All-Solid-State Batteries. In *Solid State Batteries Vol. 1: Emerging Materials and Applications*; ACS Symposium Series 1413; American Chemical Society, 2022; pp 353–393.
- (30) Payandeh, S.; Rentsch, D.; Łodziana, Z.; Asakura, R.; Bigler, L.; Černý, R.; Battaglia, C.; Remhof, A. Nido-Hydroborate-Based Electrolytes for All-Solid-State Lithium Batteries. *Adv. Funct. Mater.* **2021**, *31* (18), 2010046.
- (31) Kim, S.; Oguchi, H.; Toyama, N.; Sato, T.; Takagi, S.; Otomo, T.; Arunkumar, D.; Kuwata, N.; Kawamura, J.; Orimo, S.-i. A complex hydride lithium superionic conductor for high-energy-density all-solid-state lithium metal batteries. *Nat. Commun.* **2019**, *10* (1), 1081.
- (32) Asakura, R.; Reber, D.; Duchêne, L.; Payandeh, S.; Remhof, A.; Hagemann, H.; Battaglia, C. 4 V room-temperature all-solid-state sodium battery enabled by a passivating cathode/hydroborate solid electrolyte interface. *Energy Environ. Sci.* **2020**, *13* (12), 5048–5058.
- (33) Asakura, R.; Duchêne, L.; Payandeh, S.; Rentsch, D.; Hagemann, H.; Battaglia, C.; Remhof, A. Thermal and Electrochemical Interface Compatibility of a Hydroborate Solid Electrolyte with 3 V-Class Cathodes for All-Solid-State Sodium Batteries. *ACS Appl. Mater. Interfaces* **2021**, *13* (46), 55319–55328.
- (34) Her, J.-H.; Yousufuddin, M.; Zhou, W.; Jalisatgi, S. S.; Kulleck, J. G.; Zan, J. A.; Hwang, S.-J.; Bowman, R. C., Jr.; Udoovic, T. J. Crystal Structure of Li₂B12H12: a Possible Intermediate Species in the Decomposition of LiBH4. *Inorg. Chem.* **2008**, *47* (21), 9757–9759.
- (35) Wu, H.; Tang, W. S.; Stavila, V.; Zhou, W.; Rush, J. J.; Udoovic, T. J. Structural Behavior of Li₂B10H10. *J. Phys. Chem. C* **2015**, *119* (12), 6481–6487.
- (36) Wu, H.; Tang, W. S.; Zhou, W.; Tarver, J. D.; Stavila, V.; Brown, C. M.; Udoovic, T. J. The low-temperature structural behavior of sodium 1-carba-closo-decaborate: NaCB9H10. *J. Solid State Chem.* **2016**, *243*, 162–167.
- (37) Duchêne, L.; Kim, D. H.; Song, Y. B.; Jun, S.; Moury, R.; Remhof, A.; Hagemann, H.; Jung, Y. S.; Battaglia, C. Crystallization of closo-borate electrolytes from solution enabling infiltration into slurry-casted porous electrodes for all-solid-state batteries. *Energy Storage Mater.* **2020**, *26*, 543–549.
- (38) Tang, W. S.; Yoshida, K.; Solonin, A. V.; Skoryunov, R. V.; Babanova, O. A.; Skripov, A. V.; Dimitrieva, M.; Stavila, V.; Orimo, S.-i.; Udoovic, T. J. Stabilizing Superionic-Conducting Structures via Mixed-Anion Solid Solutions of Monocarba-closo-borate Salts. *ACS Energy Lett.* **2016**, *1* (4), 659–664.
- (39) Kim, S.; Kisu, K.; Takagi, S.; Oguchi, H.; Orimo, S.-i. Complex Hydride Solid Electrolytes of the Li(CB9H10)-Li(CB11H12) Quasi-Binary System: Relationship between the Solid Solution and Phase Transition, and the Electrochemical Properties. *ACS Appl. Energy Mater.* **2020**, *3* (5), 4831–4839.
- (40) Unemoto, A.; Yasaku, S.; Nogami, G.; Tazawa, M.; Taniguchi, M.; Matsuo, M.; Ikeshoji, T.; Orimo, S.-i. Development of bulk-type all-solid-state lithium-sulfur battery using LiBH4 electrolyte. *Appl. Phys. Lett.* **2014**, *105* (8), 083901.
- (41) Zhou, C.; Sun, H.; Wang, Q.; Grinderslev, J. B.; Liu, D.; Yan, Y.; Jensen, T. R. Highly electrochemically stable Li₂B12H12-Al₂O₃ nanocomposite electrolyte enabling A 3.8 V room-temperature all-solid-state Li-ion battery. *J. Alloys Compd.* **2023**, *938*, 168689.
- (42) Unemoto, A.; Ikeshoji, T.; Yasaku, S.; Matsuo, M.; Stavila, V.; Udoovic, T. J.; Orimo, S.-i. Stable Interface Formation between Ti₃S₂ and LiBH4 in Bulk-Type All-Solid-State Lithium Batteries. *Chem. Mater.* **2015**, *27* (15), 5407–5416.
- (43) Kim, S.; Harada, K.; Toyama, N.; Oguchi, H.; Kisu, K.; Orimo, S.-i. Room temperature operation of all-solid-state battery using a closo-type complex hydride solid electrolyte and a LiCoO₂ cathode by interfacial modification. *J. Energy Chem.* **2020**, *43*, 47–51.
- (44) Bizzotto, F.; Dachraoui, W.; Grissa, R.; Zhao, W.; Pagani, F.; Querel, E.; Kühnel, R.-S.; Battaglia, C. Modification of NMC811 with titanium for enhanced cycling and high-voltage stability. *Electrochim. Acta* **2023**, *462*, 142758.
- (45) Duchêne, L.; Lunghammer, S.; Burankova, T.; Liao, W.-C.; Embs, J. P.; Copéret, C.; Wilkening, H. M. R.; Remhof, A.; Hagemann, H.; Battaglia, C. Ionic Conduction Mechanism in the Na₂(B12H12)0.5(B10H10)0.5 closo-Borate Solid-State Electrolyte: Interplay of Disorder and Ion-Ion Interactions. *Chem. Mater.* **2019**, *31* (9), 3449–3460.
- (46) Brighi, M.; Murgia, F.; Łodziana, Z.; Schouwink, P.; Wołczyk, A.; Cerny, R. A mixed anion hydroborate/carba-hydroborate as a room temperature Na-ion solid electrolyte. *J. Power Sources* **2018**, *404*, 7–12.
- (47) Asakura, R.; Duchêne, L.; Kühnel, R.-S.; Remhof, A.; Hagemann, H.; Battaglia, C. Electrochemical Oxidative Stability of Hydroborate-Based Solid-State Electrolytes. *ACS Appl. Energy Mater.* **2019**, *2* (9), 6924–6930.
- (48) Zhao, W.; Wang, K.; Dubey, R.; Ren, F.; Brack, E.; Becker, M.; Grissa, R.; Seidl, L.; Pagani, F.; Egorov, K.; et al. Extending the high-voltage operation of Graphite/NCM811 cells by constructing a robust electrode/electrolyte interphase layer. *Mater. Today Energy* **2023**, *34*, 101301.
- (49) Deysher, G.; Chen, Y.-T.; Sayahpour, B.; Lin, S. W.-H.; Ham, S.-Y.; Ridley, P.; Cronk, A.; Wu, E. A.; Tan, D. H. S.; Doux, J.-M.; et al. Evaluating Electrolyte-Anode Interface Stability in Sodium All-Solid-State Batteries. *ACS Appl. Mater. Interfaces* **2022**, *14* (42), 47706–47715.
- (50) Asenbauer, J.; Eisenmann, T.; Kuenzel, M.; Kazzazi, A.; Chen, Z.; Bresser, D. The success story of graphite as a lithium-ion anode material - fundamentals, remaining challenges, and recent developments including silicon (oxide) composites. *Sustainable Energy Fuels* **2020**, *4* (11), 5387–5416.
- (51) Santhosha, A. L.; Medenbach, L.; Buchheim, J. R.; Adelhelm, P. The Indium-Lithium Electrode in Solid-State Lithium-Ion Batteries: Phase Formation, Redox Potentials, and Interface Stability. *Batteries Supercaps* **2019**, *2* (6), 524–529.
- (52) Jung, S. H.; Kim, U.-H.; Kim, J.-H.; Jun, S.; Yoon, C. S.; Jung, Y. S.; Sun, Y.-K. Ni-Rich Layered Cathode Materials with Electro-Chemo-Mechanically Compliant Microstructures for All-Solid-State Li Batteries. *Adv. Energy Mater.* **2020**, *10* (6), 1903360.
- (53) Lee, Y.-G.; Fujiki, S.; Jung, C.; Suzuki, N.; Yashiro, N.; Omoda, R.; Ko, D.-S.; Shiratsuchi, T.; Sugimoto, T.; Ryu, S.; et al. High-energy long-cycling all-solid-state lithium metal batteries enabled by silver-carbon composite anodes. *Nat. Energy* **2020**, *5* (4), 299–308.
- (54) Dong, B.; Yeandel, S. R.; Goddard, P.; Slater, P. R. Combined Experimental and Computational Study of Ce-Doped La₃Zr₂Li₇O₁₂ Garnet Solid-State Electrolyte. *Chem. Mater.* **2020**, *32* (1), 215–223.
- (55) Helm, B.; Schlem, R.; Wankmiller, B.; Banik, A.; Gautam, A.; Ruhl, J.; Li, C.; Hansen, M. R.; Zeier, W. G. Exploring Aliovalent

- Substitutions in the Lithium Halide Superionic Conductor $\text{Li}_3\text{xIn}_1\text{xZrxCl}_6$ ($0 \leq x \leq 0.5$). *Chem. Mater.* **2021**, *33* (12), 4773–4782.
- (56) Kraft, M. A.; Culver, S. P.; Calderon, M.; Böcher, F.; Krauskopf, T.; Senyshyn, A.; Dietrich, C.; Zevalkink, A.; Janek, J.; Zeier, W. G. Influence of Lattice Polarizability on the Ionic Conductivity in the Lithium Superionic Argyrodites $\text{Li}_6\text{PS}_5\text{X}$ ($\text{X} = \text{Cl}, \text{Br}, \text{I}$). *J. Am. Chem. Soc.* **2017**, *139* (31), 10909–10918.
- (57) Hovington, P.; Lagacé, M.; Guerfi, A.; Bouchard, P.; Mauger, A.; Julien, C. M.; Armand, M.; Zaghib, K. New Lithium Metal Polymer Solid State Battery for an Ultrahigh Energy: Nano C-LiFePO₄ versus Nano Li_{1.2}V₃O₈. *Nano Lett.* **2015**, *15* (4), 2671–2678.
- (58) Porcarelli, L.; Aboudzadeh, M. A.; Rubatat, L.; Nair, J. R.; Shaplov, A. S.; Gerbaldi, C.; Mecerreyes, D. Single-ion triblock copolymer electrolytes based on poly(ethylene oxide) and methacrylic sulfonamide blocks for lithium metal batteries. *J. Power Sources* **2017**, *364*, 191–199.
- (59) Fu, C.; Homann, G.; Grissa, R.; Rentsch, D.; Zhao, W.; Gouveia, T.; Falgayrat, A.; Lin, R.; Fantini, S.; Battaglia, C. A Polymerized-Ionic-Liquid-Based Polymer Electrolyte with High Oxidative Stability for 4 and 5 V Class Solid-State Lithium Metal Batteries. *Adv. Energy Mater.* **2022**, *12* (27), 2200412.
- (60) Park, M.-S.; Jung, Y.-C.; Kim, D.-W. Hybrid solid electrolytes composed of poly(1,4-butylene adipate) and lithium aluminum germanium phosphate for all-solid-state Li/LiNi0.6Co0.2Mn0.2O₂ cells. *Solid State Ionics* **2018**, *315*, 65–70.
- (61) Xu, Y.; Wang, K.; Zhang, X.; Ma, Y.; Peng, Q.; Gong, Y.; Yi, S.; Guo, H.; Zhang, X.; Sun, X.; et al. Improved Li-Ion Conduction and (Electro)Chemical Stability at Garnet-Polymer Interface through Metal-Nitrogen Bonding. *Adv. Energy Mater.* **2023**, *13* (14), 2204377.
- (62) Zhang, Z.; Chen, S.; Yang, J.; Wang, J.; Yao, L.; Yao, X.; Cui, P.; Xu, X. Interface Re-Engineering of Li₁₀GeP₂S₁₂ Electrolyte and Lithium anode for All-Solid-State Lithium Batteries with Ultralong Cycle Life. *ACS Appl. Mater. Interfaces* **2018**, *10* (3), 2556–2565.
- (63) Ulissi, U.; Agostini, M.; Ito, S.; Aihara, Y.; Hassoun, J. All solid-state battery using layered oxide cathode, lithium-carbon composite anode and thio-LISICON electrolyte. *Solid State Ionics* **2016**, *296*, 13–17.
- (64) Ito, S.; Fujiki, S.; Yamada, T.; Aihara, Y.; Park, Y.; Kim, T. Y.; Baek, S.-W.; Lee, J.-M.; Doo, S.; Machida, N. A rocking chair type all-solid-state lithium ion battery adopting Li₂O-ZrO₂ coated LiNi0.8Co0.15Al0.05O₂ and a sulfide based electrolyte. *J. Power Sources* **2014**, *248*, 943–950.
- (65) Zhou, L.; Zuo, T.-T.; Kwok, C. Y.; Kim, S. Y.; Assoud, A.; Zhang, Q.; Janek, J.; Nazar, L. F. High areal capacity, long cycle life 4 V ceramic all-solid-state Li-ion batteries enabled by chloride solid electrolytes. *Nat. Energy* **2022**, *7* (1), 83–93.
- (66) Asano, T.; Sakai, A.; Ouchi, S.; Sakaida, M.; Miyazaki, A.; Hasegawa, S. Solid Halide Electrolytes with High Lithium-Ion Conductivity for Application in 4 V Class Bulk-Type All-Solid-State Batteries. *Adv. Mater.* **2018**, *30* (44), 1803075.
- (67) Zhou, L.; Kwok, C. Y.; Shyamsunder, A.; Zhang, Q.; Wu, X.; Nazar, L. F. A new halospinel superionic conductor for high-voltage all solid state lithium batteries. *Energy Environ. Sci.* **2020**, *13* (7), 2056–2063.
- (68) Wang, K.; Ren, Q.; Gu, Z.; Duan, C.; Wang, J.; Zhu, F.; Fu, Y.; Hao, J.; Zhu, J.; He, L.; et al. A cost-effective and humidity-tolerant chloride solid electrolyte for lithium batteries. *Nat. Commun.* **2021**, *12* (1), 4410.
- (69) Kwak, H.; Han, D.; Lyoo, J.; Park, J.; Jung, S. H.; Han, Y.; Kwon, G.; Kim, H.; Hong, S.-T.; Nam, K.-W.; et al. New Cost-Effective Halide Solid Electrolytes for All-Solid-State Batteries: Mechanochemically Prepared Fe³⁺-Substituted Li₂ZrCl₆. *Adv. Energy Mater.* **2021**, *11* (12), 2003190.
- (70) Park, J.; Han, D.; Kwak, H.; Han, Y.; Choi, Y. J.; Nam, K.-W.; Jung, Y. S. Heat treatment protocol for modulating ionic conductivity via structural evolution of $\text{Li}_{3-x}\text{Yb}_1\text{-xMxCl}_6$ ($\text{M} = \text{Hf}^{4+}, \text{Zr}^{4+}$) new halide superionic conductors for all-solid-state batteries. *Chem. Eng. J.* **2021**, *425*, 130630.
- (71) Han, Y.; Jung, S. H.; Kwak, H.; Jun, S.; Kwak, H. H.; Lee, J. H.; Hong, S.-T.; Jung, Y. S. Single- or Poly-Crystalline Ni-Rich Layered Cathode, Sulfide or Halide Solid Electrolyte: Which Will be the Winners for All-Solid-State Batteries? *Adv. Energy Mater.* **2021**, *11* (21), 2100126.
- (72) Yan, X.; Li, Z.; Wen, Z.; Han, W. Li/Li₇La₃Zr₂O₁₂/LiFePO₄ All-Solid-State Battery with Ultrathin Nanoscale Solid Electrolyte. *J. Phys. Chem. C* **2017**, *121* (3), 1431–1435.
- (73) Ohta, S.; Kobayashi, T.; Seki, J.; Asaoka, T. Electrochemical performance of an all-solid-state lithium ion battery with garnet-type oxide electrolyte. *J. Power Sources* **2012**, *202*, 332–335.
- (74) Heubner, C.; Voigt, K.; Marcinkowski, P.; Reuber, S.; Nikolowski, K.; Schneider, M.; Partsch, M.; Michaelis, A. From Active Materials to Battery Cells: A Straightforward Tool to Determine Performance Metrics and Support Developments at an Application-Relevant Level. *Adv. Energy Mater.* **2021**, *11* (46), 2102647.